Nonequilibrium cavity QED model accounting for dipole-dipole interaction in strong-, ultrastrong-, and deep-strong-coupling regimes

Asha Devi [1,*] Sarath D. Gunapala,[2] Mark I. Stockman,[3] and Malin Premaratne [1,†]

[1]*Advanced Computing and Simulation Laboratory, Department of Electrical and Computer Systems Engineering, Monash University, Clayton, Victoria 3800, Australia*

[2]*Jet Propulsion Laboratory, California Institute of Technology, Pasadena, California 91109, USA*

[3]*Department of Physics and Astronomy, Georgia State University, Atlanta, Georgia 30303, USA*

(Received 30 January 2020; revised 23 April 2020; accepted 8 June 2020; published 6 July 2020)

We propose a generalized system of nonequilibrium cavity QED with interacting dipoles coupled to a single-mode of an electromagnetic field in strong-, ultrastrong-, and deep-strong-coupling regimes. To illustrate the applicability of the system, an extended Dicke model is developed for atoms undergoing Raman transitions between the ground states in the presence of laser fields and considering dipole-dipole interactions; the latter has been neglected in many previous works. We have studied the effect of a ferroelectric and an antiferroelectric arrangement on the phase transition for both a finite and an infinite number of dipoles. An additional superradiant phase is observed in the deep-strong-coupling regime due to influence of the dipole-dipole interaction term. A high degree of dipole-dipole entanglement occurs for the antiferroelectric arrangement in the deep-strong regime, whereas it gets disentangled quite rapidly for the ferroelectric arrangement. A sharp transition of system parameters is observed in the ultrastrong-coupling regime and beyond. The dipole-dipole interaction also influences the spectra of the system, inducing a significant shift in the peaks, and modifies the average number of photons emitted.

DOI: 10.1103/PhysRevA.102.013701

I. INTRODUCTION

Quantum electrodynamics (QED) is the physics describing light-matter interactions at the atomic level [1]. Cavity QED is a branch of QED where atoms are considered at the quantum level such as two-level atoms and their interaction with the electromagnetic mode in a cavity [2]. Historically, the Jaynes-Cummings model [3] with the rotating-wave approximation (RWA) has been considered for the light-matter interaction where the coupling strength η between the atoms and field is taken to be much smaller than the transition frequency of the atom ω_a, field mode frequency ω_c, and system losses such as decay rates of the cavity κ and spontaneous emission of the atom γ. To increase control over η, experiments using the high-Q factor cavity [4] were developed which achieved a coupling strength exceeding the parameters κ and γ. This led to the strong-coupling regime (SCR) [5–7]. In the SCR, there is a faster exchange of energy between the atom and field which is called the Rabi oscillation [8]. Recently, novel work in, for example, circuit QED [9] and solid-state semiconductors [10] has made significant advances in reaching the ultrastrong-coupling regime (USCR) [11], in which the ratio of $\eta/\omega_c \sim 0.1$ and thus η is a significant fraction of ω_c. When $\eta/\omega_c \gtrsim 1$, the deep-strong-coupling regime (DSCR) [12] is reached.

Dating back to 1954, an important phenomenon called superradiance was studied by Dicke for N excited atoms to model collective constructive emission [13,14]. This model was then extended to represent the steady-state phase transition from the normal to the superradiant phase [15,16]. A crucial characteristic of the superradiant state is that the two-level atoms become polarized and the mean value of the cavity mode attains a finite value [17]. Several studies have realized the phase transition by utilizing superfluid gas coupled to an optical cavity [18], a Raman-transition-based multilevel atom in a ring cavity [19], and a Bose-Einstein condensate in an optical resonator [20]. Novel findings such as strong atom-field entanglement for a single atom [21] and vacuum polarization in a superconducting circuit [22] have catalyzed the study of these models in the USCR and DSCR.

A wide range of work has been done based on the cavity-assisted Raman-transition model [19]. With the inclusion of an additional nonlinear atom-cavity term in the dissipative system, a Rabi model is developed for a single atom showing critical phase transition behavior [23,24]. An experimental realization [25], based on the existing proposal [19], shows that the parameters in the system can be easily and independently tunable. Similarly, Ref. [26] also explored tunability of the system parameters for a spin-1 Dicke model and its rich phase transition map for different phase regions. The work done in [27] describes the necessity of different laser beam geometries for the existing Hamiltonian of [19] and accounts for its influence on motional effects present in the system.

*asha.devi@monash.edu

†malin.premaratne@monash.edu

In line with all these works, we try to realize a system based on the contribution of the additional dipole-dipole interaction (DDI) in the four-level atom with the Raman-transition scheme [19]. In this study we consider the influence of the DDI in the phase transition, spectra, and entanglement of the system. In particular, we consider N number of multilevel atoms inside an optical cavity with a single field mode in the presence of laser fields considering Raman transitions between the ground states [28–30]. We analyze the system on the basis of ferroelectric (attractive) and antiferroelectric (repulsive) arrangements of dipoles and study the extended Dicke model with dipole-dipole interaction for the SCR, USCR, and DSCR. In the SCR the impact of DDI on the phase transition and spectra is studied in the thermodynamic limit using phase-space formalism. Going beyond the SRC to the USCR and DSCR for a finite number of dipoles, we study numerically the impact of ferroelectric (attractive) and antiferroelectric (repulsive) arrangements of dipoles on intracavity photon numbers and collective spin inversion using QUTIP [31]. The phase transition in this limit is also studied via the Wigner quasiprobability distribution.

One of the main results of our work is the finding and analysis of various entanglement stability regimes of the system considered. It is known that effects of the DDI are very pronounced in the case of the USCR and DSCR [32,33]. The influence of the DDI on the atomic spin inversion and time evolution of the mean photon number is a significant result of our work. Moreover, we find that in the deep-strong regime, an additional superradiant phase transition also becomes possible. The present study also reconfirms the atom-cavity entanglement as found in previous studies [23,34]. Such a noteworthy observation may be applicable in many distinct physical models such as microcavities consisting of organic molecules [35], in controlling coupling of nanostructure systems [36–38], and in many potential applications like quantum information processing [39], nonlinear optics [40], quantum sensing [41], and QED chemistry [42].

The paper is structured as follows. Section II provides the theoretical insight of the model and the mathematical formalism. Section III outlines the influence of the DDI in the phase transition, eigenvalue analysis, and spectra in thermodynamic limit. The system is also analyzed numerically for $N = 8$ atoms in order to check the reliability of the model. In Sec. IV we study the influence of the DDI in the entanglement, phase transition, and system parameters such as photon number and collective spin inversion in the USCR and DSCR for $N \geqslant 2$. Section V summarizes this work. Appendixes A and B cover the derivation of the effective extended Dicke Hamiltonian. The simplification of the effective Hamiltonian in the superradiant phase is given in Appendix C.

II. CAVITY QED MODEL

We consider N number of atoms inside an optical cavity of volume V and coupled to a single field mode as shown in Fig. 1. Each atom is placed a distance r_d apart from each other. The entire system is subjected to a laser field so that we can take the driving and dissipation of the system into consideration. This model is inspired by the multilevel cavity-mediated Raman-transition scheme as illustrated in [19] with the significant addition of the DDI in the system. The Hamiltonian involves the counterrotating terms otherwise neglected in the RWA. This system provides greater flexibility in tuning the laser frequencies and other effective parameters to have better control over the system.

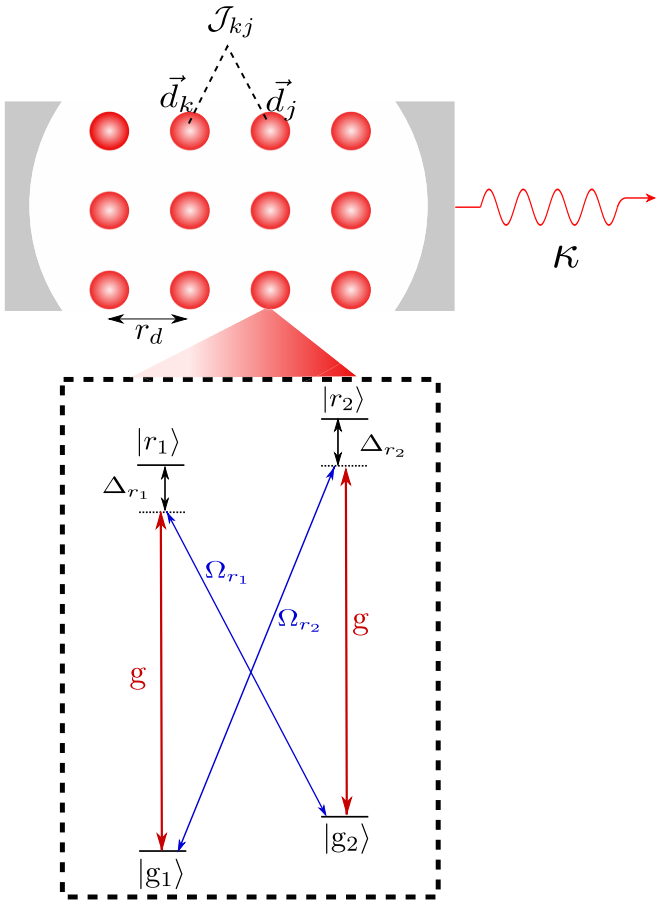

FIG. 1. Schematic of the cavity QED model with atoms separated at a distance r_d and with the DDI term $\mathcal{J}_{kj}$. The magnified view of one atom representing all shows the four-level atom with hyperfine ground levels $|g_1\rangle$ and $|g_2\rangle$ and excited states $|r_1\rangle$ and $|r_2\rangle$ (not to scale). The laser Rabi frequencies are Ω_{r_1} and Ω_{r_2} with cavity decay rate κ.

A. Closed system

We analyze the system in the presence of two laser fields which are transversely polarized to the cavity axis. A magnetic field (perpendicular to the laser field) breaks the degeneracy of the Zeeman sublevels of the atom [43]. We thus consider two ground states $|g_1\rangle$ and $|g_2\rangle$ which are mediated by a Raman transition to couple. The ground state $|g_1\rangle$ has zero energy. An atomic transition between ground states $\{|g_1\rangle$ and $|g_2\rangle\}$ and excited states $\{|r_2\rangle$ and $|r_1\rangle\}$ takes place with laser Rabi frequencies Ω_{r_2} and Ω_{r_1}, respectively. We assume an equal atom-cavity coupling strength g between $|g_1\rangle$ and $|r_1\rangle$ and also $|g_2\rangle$ and $|r_2\rangle$. The detunings from the excited states $\{|r_1\rangle, |r_2\rangle\}$ are $\{\Delta_{r_1}, \Delta_{r_2}\}$, respectively. The Hamiltonian of each dipole is

$$\hat{H}_{\rm sys} = \hat{H}_{\rm c} + \hat{H}_{\rm a} + \hat{H}_{\rm ac} + \hat{H}_{\rm la}. \tag{1}$$

The first and second terms are related to the energy of the cavity and atom, respectively, with $\hat{H}_c = \hbar\omega_q \hat{a}^\dagger \hat{a}$, where $\hat{a}^\dagger$ and $\hat{a}$ are the creation and annihilation operators of the cavity, respectively, following the commutation relation $[\hat{a}, \hat{a}^\dagger] = 1$, and

$$\hat{H}_a = \hbar\omega_{r_1}|r_1\rangle\langle r_1| + \hbar\omega_{r_2}|r_2\rangle\langle r_2| + \hbar\omega_g|g_2\rangle\langle g_2|. \quad (2)$$

The cavity frequency is denoted by ω_q and $\{\omega_{r_1}, \omega_{r_2}, \omega_g\}$ are the frequencies of the atom. The third and fourth terms of Eq. (1) are the interactions of the atom-cavity and atom-pump lasers, respectively,

$$\hat{H}_{ac} = \hbar g(\hat{a}^\dagger|g_1\rangle\langle r_1| + \hat{a}^\dagger|g_2\rangle\langle r_2|)e^{-ikx_k} + \hbar g(|r_1\rangle\langle g_1|\hat{a} + |r_2\rangle\langle g_2|\hat{a})e^{ikx_k}, \quad (3)$$

where k is the wave vector of the copropagating laser field and x_k is the location of each dipole, and

$$\hat{H}_{la} = \hbar\Omega_{r_1}[e^{i\omega_{lr_1}t}|g_2\rangle\langle r_1|e^{-ikx_k} + e^{-i\omega_{lr_1}t}|r_1\rangle\langle g_2|e^{ikx_k}] + \hbar\Omega_{r_2}[e^{i\omega_{lr_2}t}|g_1\rangle\langle r_2|e^{-ikx_k} + e^{-i\omega_{lr_2}t}|r_2\rangle\langle g_1|e^{ikx_k}]. \quad (4)$$

The pump laser frequencies are denoted by ω_{lr_1} and ω_{lr_2}. To simplify the above system, we transform $\hat{H}_{sys}$ to the interaction Hamiltonian $\hat{H}_{int}$ as

$$\hat{H}_{int} = \mathcal{U}^\dagger\{\hat{H}_{sys} - \hat{H}_0\}\mathcal{U}, \quad (5)$$

where $\mathcal{U}$ is the unitary transformation expressed as $\mathcal{U}(t) = \exp(-i\hat{H}_0 t/\hbar)$. The interaction frame rotates at the driving frequency $\frac{\omega_{lr_1}+\omega_{lr_2}}{2}$ with $\hat{H}_0$,

$$\hat{H}_0 = \frac{\hbar\omega_{lr_2}}{2}(|r_1\rangle\langle r_1| + 2|r_2\rangle\langle r_2| + \hat{a}^\dagger\hat{a}) + \frac{\hbar\omega_{lr_1}}{2}(|r_1\rangle\langle r_1| + \hat{a}^\dagger\hat{a}) + \frac{\hbar}{2}\big(\omega_{lr_2} - \omega_{lr_1}\big)|g_2\rangle\langle g_2|, \quad (6)$$

to get $\hat{H}_{int}$, which is time independent:

$$\hat{H}_{int} = \hbar\Delta_{cav}\hat{a}^\dagger\hat{a} + \hbar\Delta_{r_1}|r_1\rangle\langle r_1| + \hbar\Delta_{r_2}|r_2\rangle\langle r_2| + \hbar\Delta_{01}|g_2\rangle\langle g_2| + \hat{H}_{la}(0) + \hat{H}_{ac}. \quad (7)$$

The detunings are given as $\Delta_{cav} = \omega_q - \frac{\omega_{lr_1}+\omega_{lr_2}}{2}$, $\Delta_{r_1} = \omega_{r_1} - \frac{\omega_{lr_1}+\omega_{lr_2}}{2}$, $\Delta_{r_2} = \omega_{r_2} - \omega_{lr_2}$, and $\Delta_{01} = \omega_g - \frac{\omega_{lr_1}-\omega_{lr_2}}{2}$. When $\Delta_{r_1,r_2} \gg \{\Omega_{\{r_1,r_2\}}, g\}$, the excited states $|r_1\rangle$ and $|r_2\rangle$ will be adiabatically eliminated [19] to arrive at an effective Hamiltonian $\hat{H}_{eff}$,

$$\hat{H}_{eff} = \omega_c\hat{a}^\dagger\hat{a} + \tfrac{1}{2}\omega_0\sigma_z + \eta(\sigma_+ + \sigma_-)(\hat{a}^\dagger + \hat{a}), \quad (8)$$

with the substitutions

$$\eta = -\frac{g\Omega_{r_1}}{\Delta_{r_1}} = -\frac{g\Omega_{r_2}}{\Delta_{r_2}},$$
$$\omega_0 = \frac{\Omega_{r_2}^2}{\Delta_{r_2}} - \frac{\Omega_{r_1}^2}{\Delta_{r_2}} + \Delta_{01}, \quad (9)$$
$$\omega_c = \Delta_{cav} - \left(\frac{g^2}{\Delta_{r_1}} + \frac{g^2}{\Delta_{r_2}}\right),$$

following the derivation as given in Appendix A.

B. Dipole-dipole interaction

When the distance r_d separating two neighboring atoms is very small and the volume V of the cavity is constant, then the density of the ensemble increases [33]. In this high-density atomic cloud we cannot neglect the DDI term. The direct dipole-dipole interaction $\mathcal{J}_{kj}$ is given by

$$\mathcal{J}_{kj} = \frac{r_d^3}{4\pi}\frac{|\vec{d}_{kj}|^2 - 3(\vec{d}_{kj}\cdot\vec{e}_z)^2}{|\vec{d}_{kj}|^5}, \quad (10)$$

where $\vec{d}_{kj} = \vec{d}_k - \vec{d}_j$ corresponds to distance between the kth and jth dipoles. We assume that the dipoles are arranged along the x axis and make an angle of $\theta = 0$ with the z axis.

For weak-coupling regime, the dipole-dipole interaction term arises from the elimination of the cavity field by invoking the Born-Markov approximation [44]. However, in the case of the strong-coupling regime, rapid energy exchanges between the atom and field stop us from using the Born-Markov approximation for our model [45]. Thus, we have to resort to a different strategy in our four-level system to analyze the dipole-dipole interaction Hamiltonian

$$\hat{H}_{DD} = \hbar\sum_{k,j}^{N}\frac{\mathcal{J}_{kj}}{\nu}(\mathcal{D}_k^\dagger\mathcal{D}_j + \mathcal{D}_j^\dagger\mathcal{D}_k), \quad (11)$$

where ν is the filling factor given by Nr_d^3/V. Let us consider the case of two atoms where the operators $\mathcal{D}_1^\dagger$ and $\mathcal{D}_2$ are raising and lowering operators for atoms 1 and 2, respectively. They can be expressed as

$$\mathcal{D}_1^\dagger = g\hat{a}(|r_1\rangle\langle g_1|_1 + |r_2\rangle\langle g_2|_1),$$
$$\mathcal{D}_2 = g\hat{a}^\dagger(|g_1\rangle\langle r_1|_2 + |g_2\rangle\langle r_2|_2). \quad (12)$$

After substituting Eq. (12) in Eq. (11) one finds the expression for $\hat{H}_{DD}$, in terms of excited states $\{|r_1\rangle$ and $|r_2\rangle\}$ and ground states $\{|g_1\rangle$ and $|g_2\rangle\}$,

$$\hat{H}_{DD}^{(1,2)} = \hbar g^2\{\hat{a}|r_1\rangle\langle g_1|_1\hat{a}^\dagger|g_1\rangle\langle r_1|_2 + \hat{a}|r_1\rangle\langle g_1|_1\hat{a}^\dagger|g_2\rangle\langle r_2|_2 + \hat{a}|r_2\rangle\langle g_2|_1\hat{a}^\dagger|g_1\rangle\langle r_1|_2 + \hat{a}|r_2\rangle\langle g_2|_1\hat{a}^\dagger|g_2\rangle\langle r_2|_2 + \text{H.c.}\}, \quad (13)$$

where H.c. is the Hermitian conjugate. For the time being, we suppress the term $\sum_{k,j}^{N}\frac{\mathcal{J}_{kj}}{\nu}$, which will be added at the end.

The limit for detunings which is considered in our system is

$$\Delta_{r_1,r_2} \gg \Omega_{\{r_1,r_2\}}, g. \quad (14)$$

Under this condition, we can adiabatically eliminate the excited states. However, for interacting atoms, the DDI will lead to energy level shifts. We consider the energy level shifts to be very small in comparison to Δ_{r_1,r_2}. For such a situation to arise, the average distance between dipoles is taken to be tolerably large. We can neglect the energy level shift change surfacing due to the DDI if the detuning from the excited states is large in comparison to the atomic energy level shifts. This justifies the adiabatic elimination of the excited states. The above assumptions are only valid for pointlike dipoles such that the above condition is satisfied [46,47].

In order to derive the extended effective Hamiltonian with the DDI, as discussed in Appendix B, we find the equation of

motion of the coefficients using Eq. (13) and considering the evolution of the state of the atoms after adiabatic elimination of the excited states. Finally, Eq. (8) is extended to include the DDI to arrive at the effective extended Dicke Hamiltonian

$$\hat{H}_{\rm eff} = \hbar\omega_{\rm c}\hat{a}^\dagger\hat{a} + \hbar\omega_{\rm a}\hat{J}_z + \frac{\eta}{\sqrt{N}}\hbar(\hat{a}+\hat{a}^\dagger)(\hat{J}_+ + \hat{J}_-) + \frac{\hbar}{N\omega_{\rm c}}\eta^2\xi\hat{J}_+\hat{J}_-, \tag{15}$$

where $\hat{J}_z$, $\hat{J}_+$, and $\hat{J}_-$ are collective spin operators as defined in Eq. (B6) and ξ is the average DDI interaction term given by $\frac{1}{\nu}\sum_{k,j}^{N}\mathcal{J}_{kj} = \xi$. This system can be described in terms of an array of dipoles arranged in a different order forming a ferroelectric, i.e., attractive ($\xi < 0$) aligned dipoles and antiferroelectric, i.e., repulsive ($\xi > 0$), dipoles; $\xi = 0$ represents noninteracting dipoles. This type of model can also arise in different cases of cavity QED [33] and circuit QED [32]. We also note that there are other ways of obtaining effective Hamiltonians, e.g., by using Lie-type transformations [48].

C. Open system

The above Hamiltonian in Eq. (15) describes a closed quantum system where the associated effects of the environment or the reservoir are not yet taken into account. In an open system, the dissipation parameters such as cavity decay rates κ and spontaneous emission are included in the system as it interacts with the surrounding environment [49]. The evolution of the full system density operator $\hat{\rho}$ is expressed by the Lindblad master equation [50–52]

$$\partial_t\hat{\rho} = -\frac{i}{\hbar}[\hat{H}_{\rm eff},\hat{\rho}] + \mathcal{L}_{\rm c}\hat{\rho} + \mathcal{L}_{\rm s}\hat{\rho}. \tag{16}$$

The $\mathcal{L}_{\rm c}\hat{\rho}$ and $\mathcal{L}_{\rm s}\hat{\rho}$ include cavity decay and spontaneous emission to the environment, respectively, and are known as Lindblad superoperators. These terms have nonunitary evolution properties added to the closed system. We recall that the laser frequency is far detuned from the atomic frequency, and thus the spontaneous emission rate can be neglected [53] in our model and Eq. (16) simplifies to

$$\partial_t\hat{\rho} = -\frac{i}{\hbar}[\hat{H}_{\rm eff},\hat{\rho}] + \mathcal{L}_{\rm c}\hat{\rho}, \tag{17}$$

with $\mathcal{L}_{\rm c}\hat{\rho} = \kappa(2\hat{a}\hat{\rho}\hat{a}^\dagger - \hat{a}^\dagger\hat{a}\hat{\rho} - \hat{\rho}\hat{a}^\dagger\hat{a})$.

As an example which could illustrate the use of the proposed model described by Eqs. (15) and (17), one can consider ^{87}Rb atoms from the alkali-metal group for experimental implementations. These atoms are excited by a laser with the D_1 transition and the D_1 line $|5\,^2S_{1/2}(F_1)\rangle \leftrightarrow |5\,^2P_{1/2}(F_1')\rangle$ is a part of fine-structure doublet [19,43]. Here F_1 and F_1' are the hyperfine levels in which the ground and excited states are present. One can use $g/2\pi \approx 50$ kHz and $\kappa/2\pi \approx 20$ kHz, which leads to η having a value approximately equal to hundreds of kilohertz and with control of the detunings to reach the coupling regime $\omega_{\rm c} \sim \omega_{\rm a} \sim \eta$ [19,54]. In particular, we have used the normalized values $\omega_{\rm c} = \omega_{\rm a} = 1.0$ and $\kappa = 0.2$ for the calculations, as will be discussed in Sec. III. It should be noted that all parameters in the thermodynamic limit are on the order of kilohertz.

III. PHASE TRANSITION, EIGENVALUE ANALYSIS, AND SPECTRA

A. Phase transition

For the semiclassical analysis we intend to find the expected values of the field mode $\langle\hat{a}\rangle$, spin polarization $\langle\hat{J}_-\rangle$, and population inversion $\mathrm{Re}(\langle\hat{J}_z\rangle)$. The expected value of an operator, say, $\langle\hat{a}\rangle$, is determined by $\langle\hat{a}\rangle = \mathrm{Tr}[\hat{\rho}\hat{a}]$ and its equation of motion (EOM) with

$$\partial_t\langle\hat{a}\rangle = \partial_t\mathrm{Tr}[\hat{\rho}\hat{a}] = \mathrm{Tr}[(\partial_t\hat{\rho})\hat{a}]. \tag{18}$$

Substituting Eq. (17) in Eq. (18), we have the EOM for the field operator with the cyclic properties of the trace [55]

$$\partial_t a = -(\kappa + i\omega_{\rm c})a - i\frac{\eta}{\sqrt{N}}(J_-^* + J_-). \tag{19}$$

Similarly, we obtain the EOM for operators $\langle\hat{J}_-\rangle$ and $\langle\hat{J}_z\rangle$:

$$\begin{aligned}\partial_t J_- &= -i\omega_{\rm a}J_- + 2i\frac{\eta}{\sqrt{N}}(a+a^*)J_z - i\frac{\xi}{N\omega_{\rm c}}\eta^2 J_-,\\ \partial_t J_z &= i\frac{\eta}{\sqrt{N}}(a+a^*)(J_- - J_-^*).\end{aligned} \tag{20}$$

Here we have assumed factorization of the given operators, e.g., $\langle\hat{J}_{\pm,z}(\hat{a}+\hat{a}^\dagger)\rangle = \langle\hat{J}_{\pm,z}\rangle\langle\hat{a}+\hat{a}^\dagger\rangle$. The scalar variables appearing in above equations are $\langle\hat{a}\rangle = a$, $\langle\hat{J}_-\rangle = J_-$, and $\langle\hat{J}_z\rangle = J_z$. Solving Eqs. (19) and (20) with conservation of the total spin, $J_z^2 + |J_-|^2 = \frac{N^2}{4}$ for steady states using $\partial_t a = 0$, $\partial_t J_- = 0$, and $\partial_t J_z = 0$; we get two sets of values for different regimes of η. For $\eta > \eta_{\rm c}$,

$$a_{\rm ss} = \pm\frac{\eta\sqrt{N}}{\omega_{\rm c} - i\kappa}\sqrt{1 - \frac{1}{\eta^4}\left\{\frac{1}{2}\sqrt{\left(\omega_{\rm c} + \frac{\kappa^2}{\omega_{\rm c}}\right)\left(\omega_{\rm a} + \frac{\xi}{\omega_{\rm c}}\eta^2\right)}\right\}^4}, \tag{21a}$$

$$(J_-)_{\rm ss} = \mp\frac{N}{2}\sqrt{1 - \frac{1}{\eta^4}\left\{\frac{1}{2}\sqrt{\left(\omega_{\rm c} + \frac{\kappa^2}{\omega_{\rm c}}\right)\left(\omega_{\rm a} + \frac{\xi}{\omega_{\rm c}}\eta^2\right)}\right\}^4}, \tag{21b}$$

$$(J_z)_{\rm ss} = -\frac{N}{8}\frac{1}{\eta^2}\left(\omega_{\rm c} + \frac{\kappa^2}{\omega_{\rm c}}\right)\left(\omega_{\rm a} + \frac{\xi}{\omega_{\rm c}}\eta^2\right), \tag{21c}$$

where $a_{\rm ss}$, $(J_-)_{\rm ss}$, and $(J_z)_{\rm ss}$ represent the corresponding steady-state parameters and the critical coupling $\eta_{\rm c}$ depends on the DDI parameter ξ,

$$\eta_{\rm c} = \sqrt{\frac{-\omega_{\rm a}\omega_{\rm c}\left(\kappa^2 + \omega_{\rm c}^2\right)}{\xi\left(\kappa^2 + \omega_{\rm c}^2\right) - 4\omega_{\rm c}^2}}. \tag{22}$$

For $\eta < \eta_{\rm c}$, the steady-state parameters are $a_{\rm ss} = 0$, $(J_-)_{\rm ss} = 0$, and $(J_z)_{\rm ss} = -\frac{N}{2}$. They obtain nonvanishing finite values for $\eta > \eta_{\rm c}$, which marks the quantum phase transition from the normal to the superradiant phase [15,16,56]. In particular, we have considered $\omega_{\rm c} = \omega_{\rm a} = 1.0$, $\kappa = 0.2$, and $\xi = \{-0.5, 0.0, 0.5\}$, resulting in $\eta_{\rm c} = \{0.4797, 0.5099, 0.5467\}$, respectively. Figure 2 represents the semiclassical phase diagram depicting the variation of steady-state parameters with η. Moreover, variation of $\eta_{\rm c}$ with ξ signifies a shift in the transition point between the ferroelectric ($\xi = -0.5$) and the

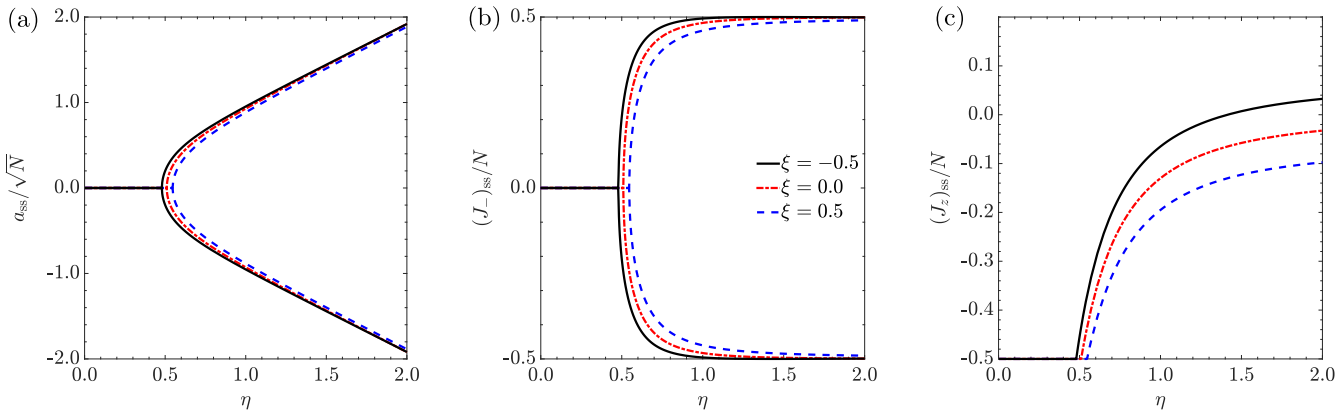

FIG. 2. Semiclassical phase diagrams plotted for $\kappa = 0.2$ and $\omega_a = \omega_c = 1.0$. Here $\eta_c = \{0.4797, 0.5099, 0.5467\}$ for $\xi = \{-0.5, 0.0, 0.5\}$, respectively.

antiferroelectric ($\xi = 0.5$) arrangement of dipoles. For ferroelectric dipoles, the phase transition is obtained earlier than for antiferroelectric dipoles.

B. Nondissipative model

As Eq. (15) cannot be solved analytically [57], we use the Holstein-Primakoff (HP) approximation [58,59] for linearization of the nondissipative case. When total excitations are small, angular momentum operators can be represented by bosonic modes, i.e., $J_z = b^\dagger b - \frac{N}{2}$, $J_+ = b^\dagger\sqrt{N - b^\dagger b}$, and $J_- = (\sqrt{N - b^\dagger b})b$, where $[b, b^\dagger] = 1$. For $N \gg 1$, the quadratic Hamiltonian in the case of a normal phase ($\eta < \eta_c$) is

$$\hat{H}_{\rm HPn} = \hbar\omega_c a^\dagger a + \hbar\omega_a b^\dagger b + \hbar\eta(a^\dagger + a)(b^\dagger + b) + \epsilon b^\dagger b, \tag{23}$$

with $\epsilon = \hbar\eta^2\xi/\omega_c$. The above equation is then diagonalized using the Bogoliubov procedure [58,60,61]. This introduces the eigenmode operators $e_\pm$ leading to the Hamiltonian $\hat{H}_{\rm HPn} = \sum_{\upsilon=\pm}\hbar\omega_\upsilon e_\upsilon^\dagger e_\upsilon$, yielding excitation frequencies

$$\omega_\pm^2 = \tfrac{1}{2}\left\{\omega_c^2 + \Omega_d^2 \pm \sqrt{\left(\omega_c^2 - \Omega_d^2\right)^2 + 16\eta^2\omega_c\omega_a}\right\}, \tag{24}$$

with $\Omega_d^2 = \omega_a(\omega_a + \epsilon)$. The excitation frequency ω_- is real for $\omega_c^2 + \Omega_d^2 \geqslant \sqrt{(\omega_c^2 - \Omega_d^2)^2 + 16\eta^2\omega_c\omega_a}$, arriving at a critical value of coupling

$$\eta_c = \sqrt{\frac{\omega_c\omega_a}{4 - \xi}}, \tag{25}$$

which can also be obtained by substituting $\kappa = 0$ in Eq. (22).

For the superradiant phase ($\eta > \eta_c$), the bosonic operators have macroscopic values and hence they undergo coherent displacement $a^\dagger = c^\dagger + \sqrt{\alpha}$ and $b^\dagger = d^\dagger - \sqrt{\beta}$, where $c^\dagger$ and $d^\dagger$ are fluctuation operators and $\{\alpha, \beta\}$ are the displacements. Using the HP approximation on Eq. (15), as discussed in Appendix C, the effective Hamiltonian for the superradiant phase can be written as

$$\hat{H}_{\rm HPs} = \hbar\omega_c c^\dagger c + \hbar\omega_1 d^\dagger d + \hbar\omega_2(d^\dagger + d)^2 + \hbar\eta_1(c^\dagger + c)(d^\dagger + d) + \text{const}, \tag{26}$$

with

$$\omega_1 = \omega_a + \frac{2\omega_a}{\varkappa(4 - \xi)}(1 - \varkappa), \tag{27a}$$

$$\omega_2 = \frac{\omega_a(1 - \varkappa)}{2\varkappa(4 - \xi)}\left\{\frac{3 + \varkappa}{1 + \varkappa} - \xi\right\}, \tag{27b}$$

$$\eta_1 = \eta\varkappa\sqrt{\frac{2}{1 + \varkappa}}, \tag{27c}$$

and $\varkappa = \frac{\eta_c^2}{\eta^2}$. Using $\varkappa = 1$ in Eq. (26), one can recover Eq. (23). These equations will be utilized in Sec. III C for eigenvalue and spectral analyses.

C. Eigenvalue and spectral analyses with DDI

In this section we present an eigenvalue analysis of the system using a Fokker-Planck equation [62]. The Fokker-Planck equation is succinctly expressed as the EOM of a probability distribution $\mathcal{P}(\phi, \varphi)$, with ϕ and φ classical forms of the quantum fluctuation operators. Such an equation also depicts information on the mean values of operators and further on the analysis of the spectra of the system. In addition, $\mathcal{P}(\phi, \varphi)$ illustrates normally ordered operators [63] using the Glauber-Sudarshan P representation [57,64,65]

$$\langle\hat{\phi}^{\dagger r}\hat{\phi}^s\hat{\varphi}^{\dagger t}\hat{\varphi}^v\rangle = \int d^2\phi\, d^2\varphi\, \mathcal{P}(\phi, \varphi)\phi^{*r}\phi^s\varphi^{*t}\varphi^v, \tag{28}$$

with $d^2\phi = d\{\text{Re}[\phi]\}d\{\text{Im}[\phi]\}$ and $d^2\varphi = d\{\text{Re}[\varphi]\}d\{\text{Im}[\varphi]\}$. For the next step, we discuss the characteristic function $\mathcal{Y}(x, y)$,

$$\mathcal{Y}(x, y) = \text{Tr}[\hat{\rho}e^{ix^*\hat{\phi}^\dagger}e^{ix\hat{\phi}}e^{iy^*\hat{\varphi}^\dagger}e^{iy\hat{\varphi}}], \tag{29}$$

with density operator $\hat{\rho}$. The EOM for $\mathcal{Y}(x, y)$ is formed using the equation $\frac{d\hat{\rho}}{dt} = \mathcal{L}\hat{\rho}$,

$$\dot{\mathcal{Y}} = \text{Tr}[\dot{\hat{\rho}}e^{ix^*\hat{\phi}^\dagger}e^{ix\hat{\phi}}e^{iy^*\hat{\varphi}^\dagger}e^{iy\hat{\varphi}}], \tag{30}$$

where $\dot{\hat{\rho}}$ is represented by Eq. (17). The equations result in the semipositive-definiteness of drift and diffusion matrices. To overcome this issue of semipositive-definiteness, we have interpreted the representation as a positive-P representation which considers the variables $\hat{\phi}^\dagger$ and $\hat{\phi}$ as complex variables instead of conjugates. A more detailed discussion can be

found in [57,66]. Utilizing these assumptions and normal ordering of operators, we obtain a Fourier transform of $\mathcal{Y}(x, y)$ to get $\mathcal{P}(\phi, \varphi)$ and finally compute the Fokker-Planck EOM

$$\frac{\partial \mathcal{P}}{\partial t} = \frac{\partial}{\partial \vartheta^\top} \mathcal{A} \vartheta \mathcal{P} + \frac{1}{2} \frac{\partial}{\partial \vartheta^\top} \mathcal{B} \frac{\partial}{\partial \vartheta} \mathcal{P}, \tag{31}$$

$\vartheta := (\phi, \phi^*, \varphi, \varphi^*)^\top$, and $\partial_\vartheta := (\partial_\phi, \partial_{\phi^*}, \partial_\varphi, \partial_{\varphi^*})^\top$ with drift matrix $\mathcal{A}$ and diffusion matrix $\mathcal{B}$ given by [57]

$$\mathcal{A} = i \begin{pmatrix} \omega_a - i\kappa & 0 & \eta_1 & \eta_1 \\ 0 & -(i\kappa + \omega_a) & -\eta_1 & -\eta_1 \\ \eta_1 & \eta_1 & \omega_1 + 2\omega_2 & 2\omega_2 \\ -\eta_1 & -\eta_1 & -2\omega_2 & -(\omega_1 + 2\omega_2) \end{pmatrix}, \tag{32a}$$

$$\mathcal{B} = i \begin{pmatrix} 0 & 0 & -\eta_1 & 0 \\ 0 & 0 & 0 & \eta_1 \\ -\eta_1 & 0 & -2\omega_2 & 0 \\ 0 & \eta_1 & 0 & 2\omega_2 \end{pmatrix}, \tag{32b}$$

valid for $\eta > \eta_c$ along with ω_1, ω_2, and η_1 as defined in Eq. (27). In the case of $\eta < \eta_c$, η_1 is replaced by η and $\omega_1 = \omega_a$ and $\omega_2 = 0$. The imaginary and real eigenvalues of the drift matrix $\mathcal{A}$ represent the excitations and damping of the system, respectively. Each of them has two parts: the photonic and atomic parts. As shown in Fig. 3, the photonic (atomic) parts are plotted using solid (dashed, dash-dotted, and dotted) lines for imaginary and real eigenvalues. We have considered $\xi = \{-0.5, 0.0, 0.5\}$ to study the effect of the arrangement of dipoles; the corresponding critical coupling constants are $\eta_c = \{0.4797, 0.5099, 0.5467\}$, which are computed using Eq. (22). The eigenvalues are unaffected by the variation of ξ for $\eta < \eta_c$, while they are highly dependent in the region $\eta \sim \eta_c$. For $\xi \geqslant 0.0$, there exists a region 1-2 where the photonic part of imaginary eigenvalues vanishes while the real part splits, as shown in the insets of the corresponding figures. In particular, the 1-2 regime is observed for $\eta = [0.9915\eta_c, 1.004\eta_c]$ for $\xi = 0.0$ and $\eta = [0.9255\eta_c, 1.0420\eta_c]$ for $\xi = 0.5$, while in the case of $\xi < 0.0$ the 1-2 regime never exists. For larger η/η_c, the photonic parts of the imaginary eigenvalues converges while the atomic part diverges for all ξ; the latter characterizes the beginning of symmetry-broken regime near $\eta/\eta_c \approx 1$ [57].

In order to probe the spectra of system we use the phase-space formalism [57,62,67]. The drift matrix $\mathcal{A}$ and diffusion matrix $\mathcal{B}$, as defined in Eqs. (32a) and (32b), carry information on the motion of the mean values and on the broadening of the distribution. We use Eq. (33) to compute the spectra $\mathcal{S}$ of the system

$$\mathcal{S}(f) = \frac{1}{2\pi} (\mathcal{A} + if\mathbf{I})^{-1} \mathcal{B} (\mathcal{A}^{\mathrm{T}} - if\mathbf{I})^{-1}, \tag{33}$$

with the frequency f and identity matrix $\mathbf{I}$.

We have studied the effect of dipole arrangement on the spectra $\mathcal{S}$. In particular, we have considered $\xi = \{-0.5, 0.0, 0.5\}$ along with $\omega_c = \omega_a = 1.0$ and $\kappa = 0.2$, as before. The spectra are plotted for $\eta/\eta_c = \{0.7, 1.0, 1.4\}$ in Figs. 4(a)–4(c), respectively. For each plot, the exterior peaks represent the atomic eigenmodes and the interior peaks

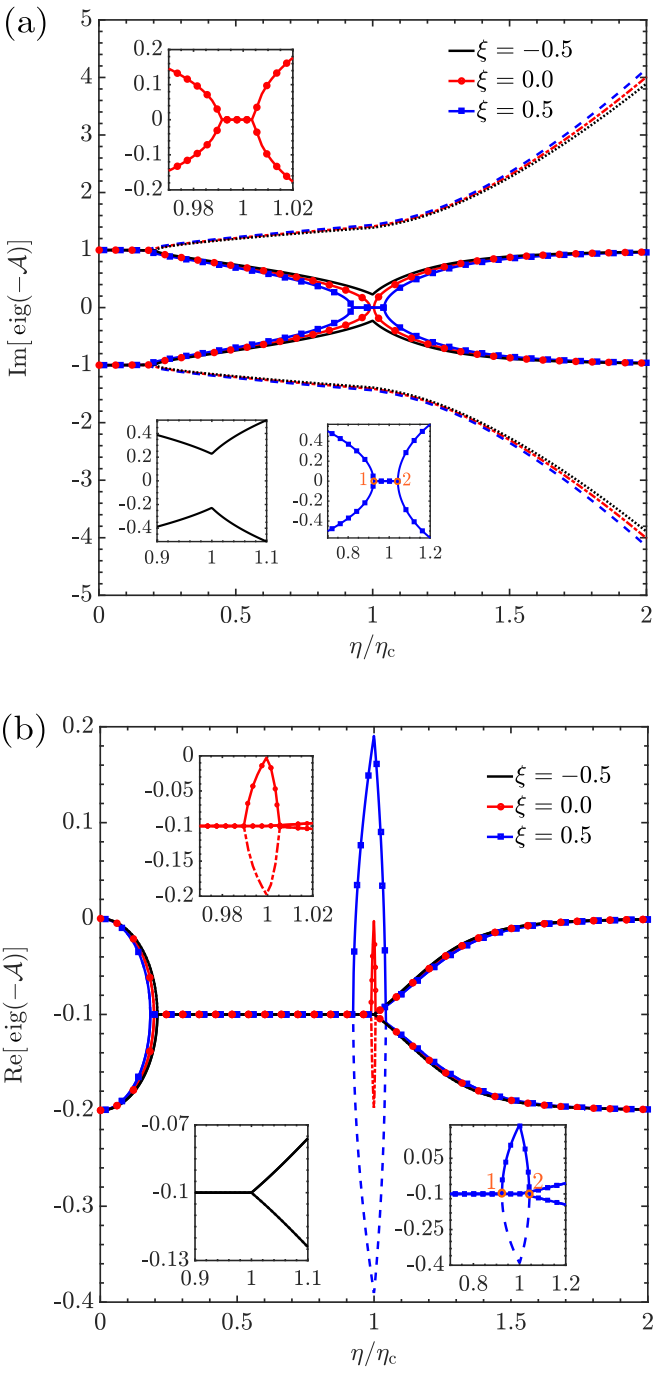

FIG. 3. (a) Imaginary eigenvalues and (b) real eigenvalues of the drift matrix $\mathcal{A}$ for different DDI values $\xi = \{-0.5, 0.0, 0.5\}$ with corresponding $\eta_c = \{0.4797, 0.5099, 0.5467\}$. The photonic (atomic) parts are plotted using solid (dashed, dash-dotted, and dotted) lines. The insets show a magnified view around $\eta = \eta_c$. The parameters are $\omega_a = \omega_c = 1.0$ and $\kappa = 0.2$.

represent the photonic eigenmodes; they are symmetric with respect to $f = 0$. The symmetrical nature of the peaks indicate the conservation of energy for any value of ξ. The amplitude of the interior peaks increases with an increase in ξ. The inner peak is found to be larger than the outer one for $\eta \leqslant \eta_c$ in Figs. 4(a) and 4(b), while it is the opposite for $\eta > \eta_c$ in Fig. 4(c). Figure 4(b) also shows that the inner peaks

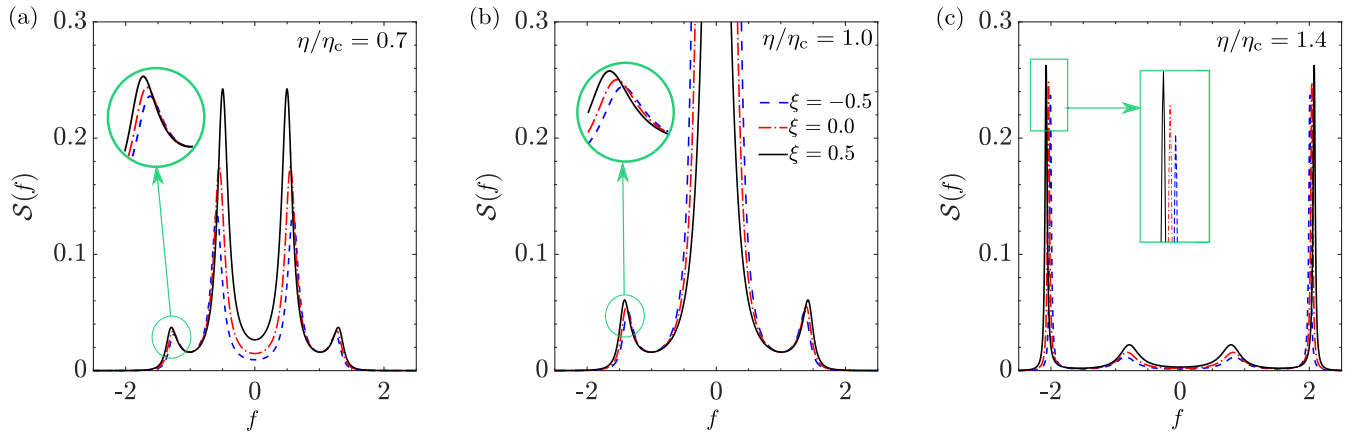

FIG. 4. For different DDI values $\xi = \{-0.5, 0.0, 0.5\}$, the spectra are plotted for different values of frequency with $\kappa = 0.2$ and $\omega_a = \omega_c = 1.0$.

converge at $\eta \sim \eta_c$, portraying the huge increase of fluctuation. Figure 4(c) demonstrates that the separation of atomic eigenmodes increases as ξ goes from negative to positive.

D. Numerical results for spectra

We consider the HP approximation to study the system analytically at the thermodynamic limit ($N \to \infty$), which provides an overall picture of the model across the phase transition as the quantum fluctuation becomes negligible in this limit. One can use the atomic coherent state representation [57] to find the analytical solution for a comparatively very large number of dipoles ($N \sim 10^3$); however, here we use the HP approximation for its mathematical simplicity. To demonstrate the validity of the effective Hamiltonian we analyze the numerical solution for comparison. Carrying out simulations in particular approximating $N \to \infty$ is computationally prohibitive and beyond the scope of this paper. As an alternative, we have obtained a numerical solution for $N = 8$. The numerical results are qualitatively similar to the analytical solution ($N \to \infty$), although we do not have an analytical expression which represents a critical value of the coupling η_c. In Fig. 5 the numerical plot for spectra is shown for $N = 8$ atoms for a small value of η. This is quite similar for the $N \to \infty$ case when $\eta < \eta_c$.

IV. INFLUENCE OF THE DDI IN THE USCR AND DSCR

Here we study the impact of the dipole-dipole interaction for a finite number of dipoles $N \geqslant 2$ in the strong-, ultrastrong-, and deep-strong-coupling regimes and beyond. Considering a very small cavity volume V, the number of dipoles can be greatly reduced [60]. Controlling the detunings, laser frequencies, and coupling parameter in a whispering-gallery-mode microtoroidal resonator [68] will lead to the ultrastrong- and deep-strong-coupling regimes. For experimental implementations, one can use $g/2\pi \simeq 200$ MHz and $\kappa/2\pi \simeq 0.2$ MHz, which results in $\eta/2\pi$ being on the order of hundreds of megahertz [23,69].

In this section we study system characteristics considering $N = 2$ for different coupling strengths. Taking the cavity losses into account in the effective system as in Eq. (17), we present the impact of ξ on the collective atomic inversion and photon number in different coupling regimes. Normalized parameters are considered for the representation with $\eta/2\pi \to \bar{\eta}$, $\kappa/2\pi \to \bar{\kappa}$, $\xi/2\pi \to \bar{\xi}$, $\omega_c/2\pi \to \bar{\omega}_c$, and $\omega_a/2\pi \to \bar{\omega}_a$. For the numerical simulation of the steady-state collective atomic inversion $\langle J_z\rangle_{ss}$ and photon number $\langle \hat{a}^\dagger \hat{a}\rangle_{ss}$, we consider $\bar{\omega}_c = \bar{\omega}_a = 1.0$, $\bar{\eta} = \{0.5, 1.0, 2.0, 2.5\}$, and $\bar{\kappa} = 0.2$. For a small range of DDI values as it changes from attractive to repulsive, there is a transition in the system behavior which is observed from variation of $\langle J_z\rangle_{ss}$ and $\langle \hat{a}^\dagger \hat{a}\rangle_{ss}$ as shown in Figs. 6(a) and 6(b), respectively. This effect becomes more prominent as $\bar{\eta}$ increases to $\bar{\eta} \gtrsim 2$, i.e., beyond the DSCR; the system becomes unstable. This signifies that the arrangement of dipoles has a stark effect in the DSCR and beyond. The steady-state photon number $\langle \hat{a}^\dagger \hat{a}\rangle$ rapidly increases with the coupling strength $\bar{\eta}$ as portrayed in Fig. 6(b).

We use the Wigner function $\mathcal{W}(\alpha)$ [70] to illustrate the above-mentioned transition-type characteristic of the system

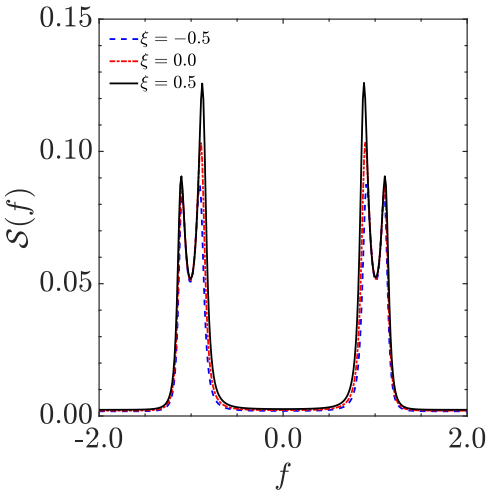

FIG. 5. For different DDI values $\xi = \{-0.5, 0.0, 0.5\}$, the numerical plot of spectra is for different values of frequency with $\kappa = 0.2$ and $\omega_a = \omega_c = 1.0$ ($\eta = 0.7$).

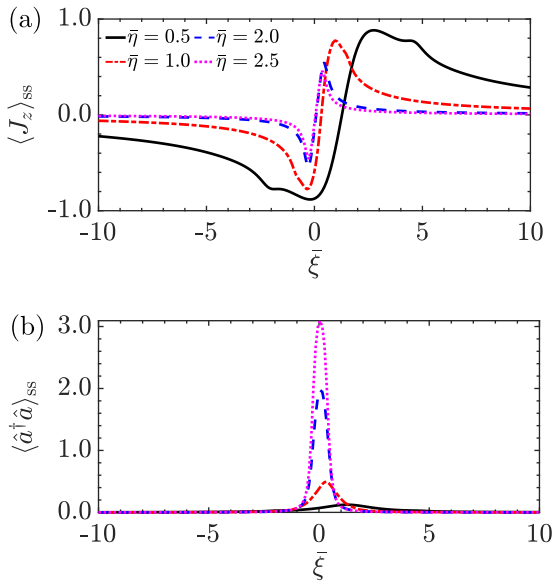

FIG. 6. Variation of (a) collective atomic inversion and (b) number of photons, plotted with different values of $\bar{\xi}$ for $N = 2$, with value of $\bar{\kappa} = 0.2$, $\bar{\omega}_a = \bar{\omega}_c = 1.0$, and $\hbar = 1$ in steady state.

around small values of $|\bar{\xi}|$. Here $\mathcal{W}(\alpha)$ is a quasiprobability distribution and is a quantum analog of the classical phase-space distribution with quantum correction [71] and is defined as

$$\mathcal{W}(\alpha) = \frac{2}{\pi} \mathrm{tr}[D^\dagger(\alpha)\hat{\rho}D(\alpha)(-1)^{\hat{a}^\dagger \hat{a}}], \tag{34}$$

with a displacement operator $D(\alpha) := \exp(\alpha\hat{a}^\dagger - \alpha^*\hat{a})$ acting on the vacuum state $|0\rangle$ of a single cavity mode to produce a coherent state $|\alpha\rangle$ with $\alpha = (x + iy)/\sqrt{2}$ [70]. Here x and y represent the displacement of the position and momentum of a quantum particle. The Wigner distribution is plotted in Fig. 7 for $N = 2$, $\bar{\eta} = 2.5$, and $\bar{\xi} = \{-0.50, -0.18, -0.14, 0.00, 0.38, 0.60\}$. Figure 7(a) represents the normal state of the system for $\bar{\xi} = -0.50$, characterized by a single peak at the center. At $\bar{\xi} = -0.18$, a superradiant transition takes place which is characterized by a slight splitting of the peak as portrayed in Fig. 7(b). This can be related to the superradiant transition in the case of the original Dicke model [23,53]. As $\bar{\xi}$ reaches -0.14, a distinctive split is observed portraying four peaks in Fig. 7(c), which characterizes the degeneracy of the system. This can also be related to the ground-state degeneracy of the cavity state of an equilibrium model [72]. For a small series of values of $\bar{\xi}$ from -0.13 to 0.38, an additional superradiant phase is formed showing strong peaks in Figs. 7(d) and 7(e). This additional phase was also observed in [23] when including a nonlinear atom-cavity term in the Rabi model. At $\bar{\xi} = 0.60$, a distinct mixed state characterized by an elongated peak along the x axis is observed, as shown in Fig. 7(f).

A. Entanglement

For an open quantum system consisting of many components, entanglement measurement has boosted interest significantly, especially with the system in proximity to a quantum phase transition [73] and in the application in quantum information processing [74]. For a mixed state we can calculate the logarithmic negativity which provides information on the upper bound of the entanglement [23]. It is defined by $\mathcal{E}_\mathcal{N} = \log_2 \|\rho^{Ts}\|_1$ based on ρ^{Ts}, which is the partial transpose of the mixed state ρ with the trace norm $\|M\|_1 := \mathrm{Tr}(\sqrt{M^\dagger M})$ [75].

In this dissipative system, we study the entanglement between dipole-cavity and dipole-dipole interactions in terms of

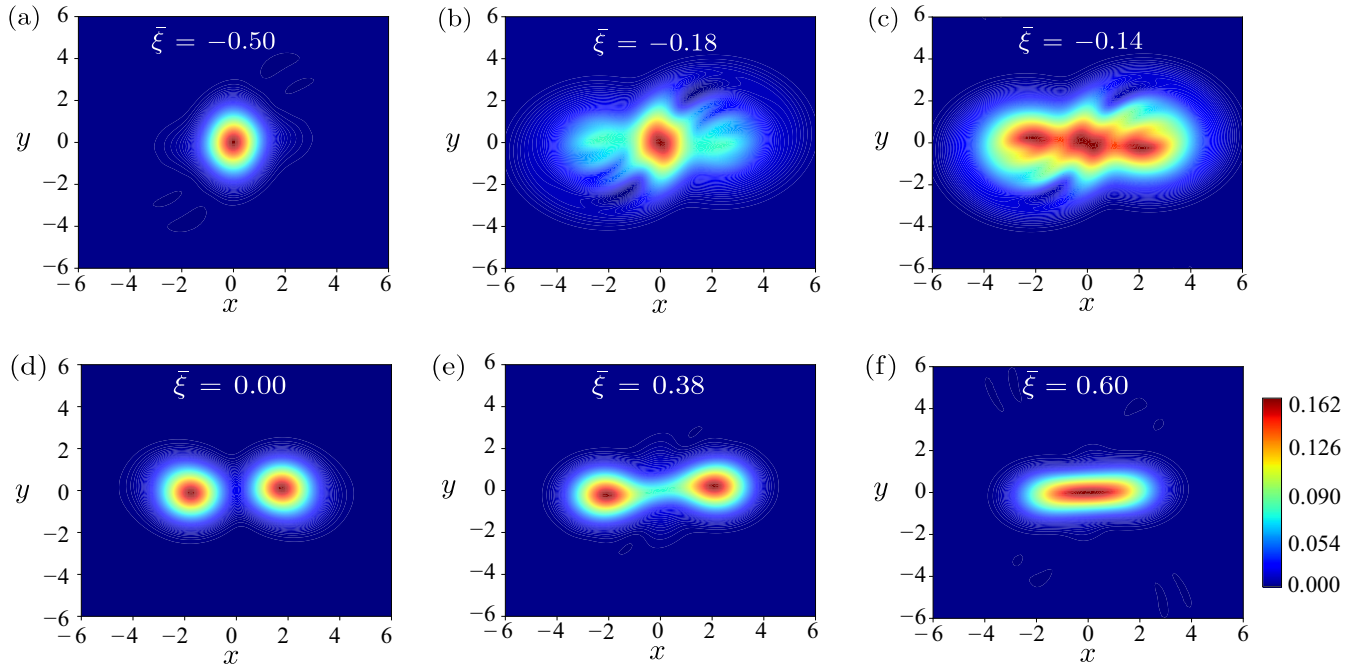

FIG. 7. Quasiprobability distribution $\mathcal{W}(\alpha)$ for different values of $\bar{\xi} = \{-0.50, -0.18, -0.14, 0.00, 0.38, 0.60\}$ and $\bar{\eta} = 2.5$, with the number of dipoles $N = 2$. The other parameters are $\bar{\omega}_c = \bar{\omega}_a = 1.0$, $\hbar = 1$, and $\bar{\kappa} = 0.2$.

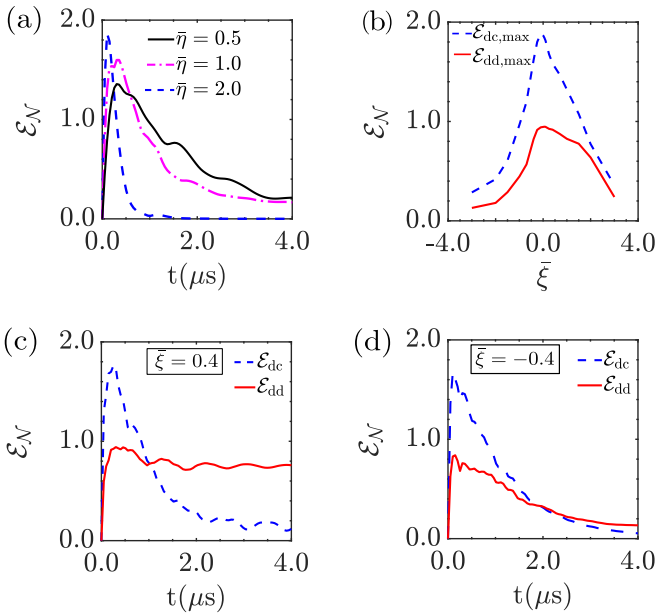

FIG. 8. Measuring entanglement. (a) Variation of logarithmic negativity $\mathcal{E}_{\mathcal{N}}$ with time to measure the dipole-cavity entanglement for different values of the coupling parameter. (b) Plot of maximum entanglement achieved for a range of DDI values $\bar{\xi} = [-3.0, 3.0]$ and $\bar{\eta} = 2.0$. Here the entanglement of all dipoles to the cavity is $\mathcal{E}_{\rm dc}$ and one dipole to the rest of the system is $\mathcal{E}_{\rm dd}$. Also plotted is the variation of entanglement for (c) repulsive DDI ($\bar{\xi} = 0.4$) and (d) attractive DDI ($\bar{\xi} = -0.4$) with time. In all plots, $N = 4$, $\bar{\eta} = 2.0$, $\bar{\omega}_{\rm a} = 0.0$, $\bar{\omega}_{\rm c} = 1.0$, $\hbar = 1$, and $\bar{\kappa} = 0.2$ are considered.

both repulsive and attractive DDIs. At time $t = 0$, we have a disentangled state $|g_2\rangle \otimes |0\rangle$. The variation of entanglement between the cavity and dipoles is measured with time for different coupling parameters $\bar{\eta} = \{0.5, 1.0, 2.0\}$ as shown in Fig. 8(a) with $\bar{\omega}_{\rm a} = 0.0$, $\bar{\omega}_{\rm c} = 1.0$, and $\bar{\kappa} = 0.2$. The system shows a high degree of entanglement after a short time $t \propto 1/\bar{\eta}$ followed by disentanglement between the dipoles and cavity, which is also in line with observations made in [23].

Next we define the entanglement between all dipoles and the cavity as $\mathcal{E}_{\rm dc}$ and one dipole with the rest of the system as $\mathcal{E}_{\rm dd}$ for both the repulsive DDI ($\bar{\xi} > 0$) and the attractive DDI ($\bar{\xi} < 0$) in Figs. 8(c) and 8(d), respectively. For the repulsive DDI, $\mathcal{E}_{\rm dd}$ does not decay with time while $\mathcal{E}_{\rm dc}$ does. Therefore, the dipole-dipole entanglement prevails with time for $\bar{\xi} > 0$ in comparison to dipole-cavity coupling which gradually becomes disentangled. This is a very important characteristic observed in the case of repulsive dipoles. However, for attractive DDIs both $\mathcal{E}_{\rm dc}$ and $\mathcal{E}_{\rm dd}$ decay. Moreover, we have recorded maximum entanglement $\{\mathcal{E}_{\rm dc}, \mathcal{E}_{\rm dd}\}$ achieved for different values of $\bar{\xi} = [-3.0, 3.0]$ as shown in Fig. 8(b). Maximum entanglement is observed for small values of $|\bar{\xi}|$ and decreases almost linearly for $\bar{\xi} > 0$ and quadratically for $\bar{\xi} < 0$.

An explanation for the observation of enhanced dipole-dipole entanglement in the case of antiferroelectric dipoles can be made from the time evolution of the photon number. The number of photons emitted in the case of antiferroelectric

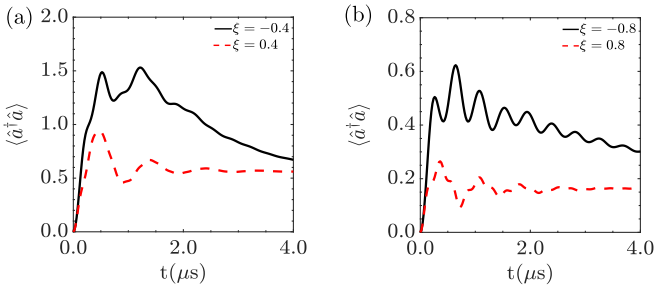

FIG. 9. Time evolution of the mean photon number $\langle \hat{a}^\dagger \hat{a} \rangle$ for (a) $N = 4$ and $\bar{\xi} = \{-0.4, 0.4\}$ and (b) $N = 8$ and $\bar{\xi} = \{-0.8, 0.8\}$. The other parameters are $\bar{\eta} = 2.0$, $\bar{\omega}_{\rm a} = 0.0$, $\bar{\omega}_{\rm c} = 1.0$, $\hbar = 1$, and $\bar{\kappa} = 0.2$.

arrangement is less than that for the ferroelectric arrangement. We explore two cases: $N = 4$ with $\bar{\xi} = \{0.4, -0.4\}$ [Fig. 9(a)] and $N = 8$ with $\bar{\xi} = \{0.8, -0.8\}$ [Fig. 9(b)]. As time passes, it can be seen that photon number of the antiferroelectric dipoles reaches a steady state at an earlier stage than in the ferroelectric case. We note that the number of photons associated with the antiferroelectric case is low in comparison to the ferroelectric case. This comparatively low number of photons in the antiferroelectric case distinguishes the dipole-dipole entanglement from the other case. Thus, we get to observe enhanced entanglement between the dipoles in the antiferroelectric arrangement as the number of photons decreases.

B. Atomic inversion

The dipole-dipole interaction has a significant effect on the time evolution of collective spin inversion $\langle J_z \rangle$. In particular, we consider an initial state $|g_1\rangle \otimes |0\rangle$ and study the effect of $\bar{\xi} = \{-0.3, 0.0, 0.5\}$ on the time evolution of $\langle J_z \rangle$ in Fig. 10. The figure demonstrates a significant effect of the DDI on the oscillations before achieving the steady state. Moreover, the time required to reach the steady state also depends

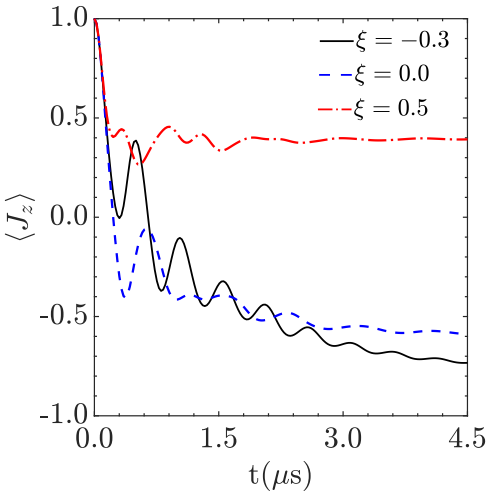

FIG. 10. Time evolution of atomic inversion plotted for $N = 8$, $\bar{\xi} = \{-0.3, 0.0, 0.5\}$, $\bar{\omega}_{\rm c} = \bar{\omega}_{\rm a} = 1.0$, $\hbar = 1$, $\bar{\kappa} = 0.2$, and $\bar{\eta} = 2.0$.

on the particular value of $\bar{\xi}$. This is a signature of a system having critical transitions [23].

V. CONCLUSION

To summarize, a generalized open cavity QED system with atoms undergoing Raman transitions with the addition of a dipole-dipole interaction was studied for strong-, ultrastrong-, and deep-strong-coupling regimes. Multilevel atoms were considered to have better control over the system parameters and to achieve different coupling regimes. It was found that the impact of the DDI increases with an increase of atom-cavity coupling and hence it cannot be ignored. The phase transition was analyzed for $N \to \infty$ and a finite number of dipoles with ferroelectric and antiferroelectric arrangements, which shows a modification of the value of the critical coupling parameter with the DDI. The spectra of the system in the thermodynamic limit were studied using phase-space formalism for strong coupling and it was found that the DDI alters the position and amplitude of the peaks. A sharp transition for collective atomic inversion and photon numbers for a very small value of the DDI was noted. The system showed a high degree of entanglement after a short time $t \propto \eta^{-1}$ followed by disentanglement between the dipoles and cavity. A strong dipole-dipole entanglement was observed for the antiferroelectric arrangement, while for the ferroelectric arrangement it became disentangled quite rapidly with time. An additional superradiant phase was observed in the DSCR with the DDI value changing from very small repulsive to attractive. Though this scheme was built from many approximations, the results of this work will provide opportunities for different physical setups of a cavity QED system [18,76].

ACKNOWLEDGMENTS

A.D. would like to thank the members of AχL at Monash University for their encouragement and support. The work of A.D. was supported by the Monash University Institute of Graduate Research. We appreciate very helpful discussions with Daniele De Bernardis (TU Wien, Austria) and Dr. Felipe Dimer de Oliveira (University of Western Australia).

APPENDIX A: DERIVATION OF EFFECTIVE HAMILTONIAN WITHOUT DDI

We introduce the evolution of the state vector $|\Psi(t)\rangle$ and its decomposition as [57]

$$|\Psi(t)\rangle = \sum_{m=0}^{\infty} \left[\left(b_{r_1}^m |r_1\rangle + b_{r_2}^m |r_2\rangle + b_{g_2}^m |g_2\rangle + b_{g_1}^m |g_1\rangle \right) \otimes |m\rangle \right], \tag{A1}$$

with the cavity mode being in the state $|m\rangle$ and the coefficients being time dependent. Substituting Eqs. (A1) and (7) into the Schrödinger equation

$$i\frac{d|\Psi(t)\rangle}{\mathrm{d}t} = \frac{1}{\hbar}\hat{H}|\Psi\rangle, \tag{A2}$$

we derive the EOM for the coefficients after neglecting the term $\hbar\Delta_{\mathrm{cav}}\hat{a}^\dagger\hat{a}$ as

$$i\dot{b}_{r_1}^m = \Delta_{r_1} b_{r_1}^m + \left(\Omega_{r_1} b_{g_2}^m + g b_{g_1}^{m+1}\sqrt{m+1}\right)e^{ikx}, \tag{A3a}$$

$$i\dot{b}_{r_2}^m = \Delta_{r_2} b_{r_2}^m + \left(\Omega_{r_2} b_{g_1}^m + g b_{g_2}^{m+1}\sqrt{m+1}\right)e^{ikx}, \tag{A3b}$$

$$i\dot{b}_{g_2}^m = \Delta_{01} b_{g_2}^m + \left(\Omega_{r_1} b_{r_1}^m + g b_{r_2}^{m-1}\sqrt{m}\right)e^{-ikx}, \tag{A3c}$$

$$i\dot{b}_{g_1}^m = \left(\Omega_{r_2} b_{r_2}^m + g b_{r_1}^{m-1}\sqrt{m}\right)e^{-ikx}. \tag{A3d}$$

When $\Delta_{r_1,r_2} \gg \{\Omega_{\{r_1,r_2\}}, g_{\{r_1,r_2\}}\}$, the excited states $|r_1\rangle$ and $|r_2\rangle$ can be adiabatically eliminated. Noting that $\dot{b}_{r_1}^m$ and $\dot{b}_{r_2}^m$ evolve to zero, Eqs. (A3a) and (A3b) can be approximated as

$$\begin{aligned} b_{r_1}^m &= -\frac{e^{ikx}}{\Delta_{r_1}}\left(\Omega_{r_1} b_{g_2}^m + g b_{g_1}^{m+1}\sqrt{m+1}\right), \\ b_{r_2}^m &= -\frac{e^{ikx}}{\Delta_{r_2}}\left(\Omega_{r_2} b_{g_1}^m + g b_{g_2}^{m+1}\sqrt{m+1}\right). \end{aligned} \tag{A4}$$

The resulting expressions for $b_{r_1}^m$ and $b_{r_2}^m$ can be substituted in Eqs. (A3c) and (A3d) to get

$$i\dot{b}_{g_2}^m = \left(\Delta_{01} - \frac{\Omega_{r_1}^2}{\Delta_{r_1}}\right) b_{g_2}^m - \frac{g\Omega_{r_1}}{\Delta_{r_1}}\sqrt{m+1}\, b_{g_1}^{m+1} - \frac{g\Omega_{r_2}}{\Delta_{r_2}}\sqrt{m}\, b_{g_1}^{m-1} - \frac{g^2}{\Delta_{r_2}} b_{g_2}^m m, \tag{A5a}$$

$$i\dot{b}_{g_1}^m = -\frac{\Omega_{r_2}^2}{\Delta_{r_2}} b_{g_1}^m - \frac{g\Omega_{r_2}}{\Delta_{r_2}}\sqrt{m+1}\, b_{g_2}^{m+1} - \frac{g\Omega_{r_1}}{\Delta_{r_1}}\sqrt{m}\, b_{g_2}^{m-1} - \frac{g^2}{\Delta_{r_1}} b_{g_1}^m m. \tag{A5b}$$

The associated effective Hamiltonian with only the hyperfine ground states $|g_1\rangle$ and $|g_2\rangle$ has the form

$$\hat{H}_{\text{eff}} = \left(\Delta_{01} - \frac{\Omega_{r_1}^2}{\Delta_{r_1}}\right)|g_2\rangle\langle g_2| - \frac{g\Omega_{r_1}}{\Delta_{r_1}}\left(\sigma_+\hat{a} + \sigma_-\hat{a}^\dagger\right) - \frac{g\Omega_{r_2}}{\Delta_{r_2}}\left(\sigma_-\hat{a} + \sigma_+\hat{a}^\dagger\right) - \frac{\Omega_{r_2}^2}{\Delta_{r_2}}|g_1\rangle\langle g_1| - \frac{g^2}{\Delta_{r_2}}\hat{a}^\dagger\hat{a}|g_2\rangle\langle g_2| - \frac{g^2}{\Delta_{r_1}}\hat{a}^\dagger\hat{a}|g_1\rangle\langle g_1|, \tag{A6}$$

with

$$\sigma_+ = |g_2\rangle\langle g_1|, \quad \sigma_- = |g_1\rangle\langle g_2|. \tag{A7}$$

The terms $|g_1\rangle\langle g_1|$ and $|g_2\rangle\langle g_2|$ in Eq. (A6) can be redefined with σ_z and $\mathbf{1}$ and written in the form

$$|g_2\rangle\langle g_2| = \frac{\mathbf{1} + \sigma_z}{2}, \quad |g_1\rangle\langle g_1| = \frac{\mathbf{1} - \sigma_z}{2}. \tag{A8}$$

We discard the constant terms in the above Hamiltonian to arrive at the Hamiltonian given in Eq. (8).

APPENDIX B: EXTENDED EFFECTIVE HAMILTONIAN WITH THE DDI

In order to derive the extended effective Hamiltonian with the DDI, we take into account the state of the atom. The first atom (atom 1) is in the excited state and the second atom (atom 2) is in the ground state and vice versa [77],

$$|\Psi(t)_{\text{d}}\rangle = \sum_{m=0}^{\infty}\Big\{\Big[\left(b_{r_1}^m b_{g_1}^m |r_1\rangle_1|g_1\rangle_2 - b_{g_1}^m b_{r_1}^m |g_1\rangle_1|r_1\rangle_2\right) + \left(b_{r_2}^m b_{g_2}^m |r_2\rangle_1|g_2\rangle_2 - b_{g_2}^m b_{r_2}^m |g_2\rangle_1|r_2\rangle_2\right)\Big] \otimes |m\rangle\Big\}. \tag{B1}$$

The coefficients of the excited and ground states of both atoms are equal, i.e., the coefficients of $|r_1\rangle_1$ and $|r_1\rangle_2$ are the same, and the equations of the coefficients are as given in Appendix A. Following Appendix A, and taking Eq. (A2) and replacing $\hat{H}$ by $\hat{H}_{\text{DD}}^{(1,2)}$ as given in Eq. (13), we get the equations of motion for new coefficients

$$i\dot{b}_{g_1}b_{g_2}^m = \frac{g\Omega_{r_1}}{\Delta_{r_1}}\frac{g\Omega_{r_2}}{\Delta_{r_2}}[\hat{a}(\sigma_+)^{(1)}\hat{a}^\dagger(\sigma_-)^{(2)}] + \frac{g^2}{\Delta_{r_1}}\frac{g^2}{\Delta_{r_2}}[(\sigma_-)^{(2)}\hat{a}^\dagger\hat{a}^\dagger\hat{a}(|g_1\rangle\langle g_1|)^{(1)}], \tag{B2a}$$

$$i\dot{b}_{g_2}b_{g_1}^m = \frac{g\Omega_{r_2}}{\Delta_{r_2}}\frac{g\Omega_{r_1}}{\Delta_{r_1}}[\hat{a}(\sigma_-)^{(1)}\hat{a}^\dagger(\sigma_+)^{(2)}] + \frac{g^2}{\Delta_{r_2}}\frac{g^2}{\Delta_{r_1}}[(\sigma_+)^{(2)}\hat{a}^\dagger\hat{a}^\dagger\hat{a}(|g_2\rangle\langle g_2|)^{(1)}], \tag{B2b}$$

$$i\dot{b}_{g_1}b_{g_2}^m = -\frac{g\Omega_{r_1}}{\Delta_{r_1}}\frac{g\Omega_{r_2}}{\Delta_{r_2}}[\hat{a}^\dagger(\sigma_-)^{(1)}\hat{a}(\sigma_+)^{(2)}] - \frac{g^2}{\Delta_{r_1}}\frac{g^2}{\Delta_{r_2}}[(\sigma_-)^{(1)}\hat{a}^\dagger\hat{a}^\dagger\hat{a}(|g_1\rangle\langle g_1|)^{(2)}], \tag{B2c}$$

$$i\dot{b}_{g_2}b_{g_1}^m = -\frac{g\Omega_{r_2}}{\Delta_{r_2}}\frac{g\Omega_{r_1}}{\Delta_{r_1}}[\hat{a}^\dagger(\sigma_+)^{(1)}\hat{a}(\sigma_-)^{(2)}] - \frac{g^2}{\Delta_{r_2}}\frac{g^2}{\Delta_{r_1}}[(\sigma_+)^{(1)}\hat{a}^\dagger\hat{a}^\dagger\hat{a}(|g_2\rangle\langle g_2|)^{(2)}]. \tag{B2d}$$

As explained in Appendix A, $\dot{b}_{r_1}^m$ and $\dot{b}_{r_2}^m$ are assumed to be zero. The above equations contain terms involving only $|g_1\rangle\langle g_2|$, $|g_2\rangle\langle g_1|$, $|g_1\rangle\langle g_1|$, and $|g_2\rangle\langle g_2|$, i.e., only the hyperfine ground states. By putting Eq. (A8) in Eq. (B2) and adding all the terms we obtain the dipole-dipole Hamiltonian

$$\hat{H}_{\text{DD}}^{\text{eff}(1,2)} = \frac{g\Omega_{r_1}}{\omega_{\text{c}}\Delta_{r_1}}\frac{g\Omega_{r_2}}{\Delta_{r_2}}[\hat{a}\hat{a}^\dagger(\sigma_+)^1(\sigma_-)^2 - \hat{a}^\dagger\hat{a}(\sigma_-)^1(\sigma_+)^2] + \frac{g\Omega_{r_2}}{\omega_{\text{c}}\Delta_{r_2}}\frac{g\Omega_{r_1}}{\Delta_{r_1}}[\hat{a}\hat{a}^\dagger(\sigma_-)^1(\sigma_+)^2 - \hat{a}^\dagger\hat{a}(\sigma_+)^1(\sigma_-)^2]. \tag{B3}$$

With the help of the bosonic commutation relation $[\hat{a}, \hat{a}^\dagger] = 1$ and the relation as given in Eq. (9) we finally have

$$\hat{H}_{\text{DD}}^{\text{eff}(1,2)} = \frac{\eta^2}{\omega_{\text{c}}}[(\sigma_+)^1(\sigma_-)^2 + (\sigma_-)^1(\sigma_+)^2]. \tag{B4}$$

The above equation can be written including the direct dipole-dipole interaction term for all atoms, which we have omitted before:

$$\hat{H}_{\text{DD}}^{\text{eff}} = \frac{\eta^2}{\omega_{\text{c}}\nu}\sum_{k,j}^{N}\mathcal{J}_{kj}[(\sigma_+)^k(\sigma_-)^j + (\sigma_-)^k(\sigma_+)^j]. \tag{B5}$$

For an ensemble of N atoms, we rewrite η in terms of $\eta/\sqrt{N}$ and the collective spin operators as

$$\hat{J}_z = \sum_{j,k=1}^{N}\sigma_z^{(j,k)}, \quad \hat{J}_+ = \sum_{j,k=1}^{N}\sigma_+^{(j,k)}, \quad \hat{J}_- = \sum_{j,k=1}^{N}\sigma_-^{(j,k)}. \tag{B6}$$

In order for us to have a qualitative understanding of the overall system we can reduce this complex system to a more simplified one. The influence of direct dipole-dipole interaction term can be captured with an all-to-all dipole interaction in the homogeneous sample [33]

$$\frac{1}{\nu}\sum_{k,j}^{N}\mathcal{J}_{kj}[(\sigma_+)_k(\sigma_-)_j+(\sigma_-)_k(\sigma_+)_j]\rightarrow\xi\hat{J}_+\hat{J}_-. \tag{B7}$$

Here ξ is the average DDI term given by

$$\frac{1}{\nu}\sum_{k,j}^{N}\mathcal{J}_{kj}=\xi. \tag{B8}$$

We can also consider using the term $\hat{J}_-\hat{J}_+$ instead of $\hat{J}_+\hat{J}_-$, but this will lead to an imaginary value for the critical coupling described in Sec. III A. Thus, we make a seemingly justifiable decision to retain a real coupling coefficient. It is also important to note that as Eqs. (A7) and (A8) are used to represent the operators we cannot replace $\hat{J}_+\hat{J}_-$ with the atomic inversion term $\hat{J}_z$. Thus, replacing the exact DDI with the average term ξ in Eq. (B5), we get

$$\hat{H}_{\rm DD}^{\rm eff}=\frac{\hbar}{N\omega_{\rm c}}\eta^2\xi\hat{J}_+\hat{J}_-. \tag{B9}$$

Combining Eq. (B9) with Eq. (8) in the collective form gives us the effective extended Dicke Hamiltonian with the DDI:

$$\begin{aligned}\hat{H}_{\rm eff}&=\hbar\omega_{\rm c}\hat{a}^\dagger\hat{a}+\hbar\omega_{\rm a}\hat{J}_z+\frac{\eta}{\sqrt{N}}\hbar(\hat{a}+\hat{a}^\dagger)(\hat{J}_++\hat{J}_-)\\&\quad+\frac{\hbar}{N\omega_{\rm c}}\eta^2\xi\hat{J}_+\hat{J}_-.\end{aligned} \tag{B10}$$

APPENDIX C: EFFECTIVE HAMILTONIAN IN THE SUPERRADIANT PHASE

Based on the Holstein-Primakoff approximation, we describe the system in the superradiant phase. Using the displacements $a^\dagger=c^\dagger+\sqrt{\alpha}$ and $b^\dagger=d^\dagger-\sqrt{\beta}$, where $c^\dagger$ and $d^\dagger$ are fluctuation operators, in the Hamiltonian (15), we have [58]

$$\begin{aligned}\hat{H}_{\rm HPs}&=\hbar\omega_{\rm c}\{c^\dagger c+\sqrt{\alpha}(c^\dagger+c)+\alpha\}+\hbar\omega_{\rm a}\left\{d^\dagger d-\sqrt{\beta}(d^\dagger+d)+\beta-\frac{N}{2}\right\}\\&\quad+\hbar\eta\sqrt{\frac{k}{N}}(c^\dagger+c+2\sqrt{\alpha})(d^\dagger\sqrt{\varrho}+\sqrt{\varrho}d-2\sqrt{\beta}\sqrt{\varrho})+\frac{\hbar k}{\omega_{\rm c}N}\eta^2\xi\{(d^\dagger-\sqrt{\beta})\varrho(d-\sqrt{\beta})\},\end{aligned} \tag{C1}$$

with $\sqrt{\varrho}\equiv\sqrt{1-\frac{d^\dagger d-\sqrt{\beta}(d^\dagger+d)}{k}}$ and $k\equiv N-\beta$. Considering the thermodynamic limit, we can write

$$\begin{aligned}\hat{H}_{\rm HPs}&=\hbar\omega_{\rm c}c^\dagger c+\hbar\left\{\omega_{\rm a}+\frac{2\eta}{k}\sqrt{\frac{\alpha\beta k}{N}}\right\}d^\dagger d-\hbar\left\{2\eta\sqrt{\frac{\beta k}{N}}-\omega_{\rm c}\sqrt{\alpha}\right\}(c^\dagger+c)\\&\quad+\hbar\left\{\frac{4\eta}{k}\sqrt{\frac{\alpha k}{N}}\left(\frac{N}{2}-\beta\right)-\omega_{\rm a}\sqrt{\beta}-\frac{\eta^2\xi\sqrt{\beta}}{N\omega_{\rm c}}(k-\beta)\right\}(d^\dagger+d)\\&\quad+\hbar\left\{\frac{\eta}{2k^2}\sqrt{\frac{\alpha\beta k}{N}}(2k+\beta)-\frac{\eta^2\xi\beta}{N\omega_{\rm c}}\right\}(d^\dagger+d)^2+\left\{\frac{2\hbar\eta}{k}\sqrt{\frac{k}{N}}\left(\frac{N}{2}-\beta\right)\right\}(c^\dagger+c)(d^\dagger+d)\\&\quad+\hbar\left\{\omega_{\rm a}\left(\beta-\frac{N}{2}\right)+\omega_{\rm c}\alpha-\frac{\eta}{k}\sqrt{\frac{\alpha\beta k}{N}}(1+4k)+\frac{\eta^2\xi\beta}{N\omega_{\rm c}}(1+k)\right\}.\end{aligned} \tag{C2}$$

Removing terms from the above Hamiltonian which are linear in $\{c,c^\dagger,d,d^\dagger\}$, we get

$$\begin{aligned}2\eta\sqrt{\frac{\beta k}{N}}-\omega_{\rm c}\sqrt{\alpha}&=0,\\\left\{\frac{8\eta^2}{\omega_{\rm c}N}\left(\frac{N}{2}-\beta\right)-\omega_{\rm a}-\frac{\eta^2\xi}{\omega_{\rm c}N}(k-\beta)\right\}\sqrt{\beta}&=0.\end{aligned} \tag{C3}$$

The nontrivial solution is

$$\sqrt{\alpha}=\frac{\eta}{\omega_{\rm c}}\sqrt{N(1-\varkappa^2)},\quad\sqrt{\beta}=\sqrt{\frac{N}{2}(1-\varkappa)}, \tag{C4}$$

with the definition $\varkappa = \frac{\eta_c^2}{\eta^2}$. The effective Hamiltonian of Eq. (C2) becomes

$$\hat{H}_{\mathrm{HPs}} = \hbar\omega_c c^\dagger c + \hbar\left[\omega_a + \frac{2\omega_a}{\varkappa(4-\xi)}(1-\varkappa)\right] d^\dagger d + \hbar\left[\frac{\omega_a(1-\varkappa)}{2\varkappa(4-\xi)}\left\{\frac{3+\varkappa}{1+\varkappa} - \xi\right\}\right](d^\dagger + d)^2 + \hbar\eta\varkappa\sqrt{\frac{2}{1+\varkappa}}(c^\dagger + c)(d^\dagger + d) + \mathrm{const.} \tag{C5}$$

[1] D. Craig and T. Thirunamachandran, *Molecular Quantum Electrodynamics* (Dover, New York, 1998).
[2] S. Haroche and J.-M. Raimond, *Exploring the Quantum: Atoms, Cavities, and Photons* (Oxford University Press, Oxford, 2006).
[3] E. T. Jaynes and F. W. Cummings, Proc. IEEE **51**, 89 (1963).
[4] Y. Kaluzny, P. Goy, M. Gross, J. M. Raimond, and S. Haroche, Phys. Rev. Lett. **51**, 1175 (1983).
[5] J.-M. Raimond, M. Brune, and S. Haroche, Rev. Mod. Phys. **73**, 565 (2001).
[6] H. Wu, J. Gea-Banacloche, and M. Xiao, Phys. Rev. A **80**, 033806 (2009).
[7] K. Gettapola, H. Hapuarachchi, M. I. Stockman, and M. Premaratne, J. Phys.: Condens. Matter **32**, 125301 (2020).
[8] R. J. Thompson, G. Rempe, and H. J. Kimble, Phys. Rev. Lett. **68**, 1132 (1992).
[9] A. Blais, R.-S. Huang, A. Wallraff, S. M. Girvin, and R. J. Schoelkopf, Phys. Rev. A **69**, 062320 (2004).
[10] G. Günter, A. A. Anappara, J. Hees, A. Sell, G. Biasiol, L. Sorba, S. De Liberato, C. Ciuti, A. Tredicucci, A. Leitenstorfer *et al.*, Nature (London) **458**, 178 (2009).
[11] C. Ciuti, G. Bastard, and I. Carusotto, Phys. Rev. B **72**, 115303 (2005).
[12] J. Casanova, G. Romero, I. Lizuain, J. J. Garcia-Ripoll, and E. Solano, Phys. Rev. Lett. **105**, 263603 (2010).
[13] R. H. Dicke, Phys. Rev. **93**, 99 (1954).
[14] M. Gross and S. Haroche, Phys. Rep. **93**, 301 (1982).
[15] K. Hepp and E. H. Lieb, Ann. Phys. (NY) **76**, 360 (1973).
[16] F. Hioe, Phys. Rev. A **8**, 1440 (1973).
[17] B. M. Garraway, Philos. Trans. R. Soc. A **369**, 1137 (2011).
[18] K. Baumann, C. Guerlin, F. Brennecke, and T. Esslinger, Nature (London) **464**, 1301 (2010).
[19] F. Dimer, B. Estienne, A. S. Parkins, and H. J. Carmichael, Phys. Rev. A **75**, 013804 (2007).
[20] D. Nagy, G. Szirmai, and P. Domokos, Phys. Rev. A **84**, 043637 (2011).
[21] S. Ashhab and F. Nori, Phys. Rev. A **81**, 042311 (2010).
[22] M. Bamba, K. Inomata, and Y. Nakamura, Phys. Rev. Lett. **117**, 173601 (2016).
[23] A. L. Grimsmo and S. Parkins, Phys. Rev. A **87**, 033814 (2013).
[24] A. Grimsmo and A. Parkins, J. Phys. B **46**, 224012 (2013).
[25] M. P. Baden, K. J. Arnold, A. L. Grimsmo, S. Parkins, and M. D. Barrett, Phys. Rev. Lett. **113**, 020408 (2014).
[26] Z. Zhiqiang, C. H. Lee, R. Kumar, K. J. Arnold, S. J. Masson, A. S. Parkins, and M. D. Barrett, Optica **4**, 424 (2017).
[27] Z. Zhang, C. H. Lee, R. Kumar, K. J. Arnold, S. J. Masson, A. L. Grimsmo, A. S. Parkins, and M. D. Barrett, Phys. Rev. A **97**, 043858 (2018).
[28] M. G. Raymer and J. Mostowski, Phys. Rev. A **24**, 1980 (1981).
[29] K. Drühl, R. G. Wenzel, and J. L. Carlsten, Phys. Rev. Lett. **51**, 1171 (1983).
[30] T. Wilk, H. P. Specht, S. C. Webster, G. Rempe, and A. Kuhn, J. Mod. Opt. **54**, 1569 (2007).
[31] J. R. Johansson, P. D. Nation, and F. Nori, Comput. Phys. Commun. **184**, 1234 (2013).
[32] T. Jaako, Z.-L. Xiang, J. J. Garcia-Ripoll, and P. Rabl, Phys. Rev. A **94**, 033850 (2016).
[33] D. De Bernardis, T. Jaako, and P. Rabl, Phys. Rev. A **97**, 043820 (2018).
[34] N. Lambert, C. Emary, and T. Brandes, Phys. Rev. Lett. **92**, 073602 (2004).
[35] S. Kéna-Cohen, S. A. Maier, and D. D. Bradley, Adv. Opt. Mater. **1**, 827 (2013).
[36] B. Liu, W. Zhu, S. D. Gunapala, M. I. Stockman, and M. Premaratne, ACS Nano **11**, 12573 (2017).
[37] C. Jayasekara, M. Premaratne, S. D. Gunapala, and M. I. Stockman, J. Appl. Phys. **119**, 133101 (2016).
[38] W. Zhu, I. D. Rukhlenko, and M. Premaratne, J. Opt. Soc. Am. B **29**, 2659 (2012).
[39] A. F. Kockum, A. Miranowicz, S. De Liberato, S. Savasta, and F. Nori, Nat. Rev. Phys. **1**, 19 (2019).
[40] S. Felicetti, D. Z. Rossatto, E. Rico, E. Solano, and P. Forn-Diaz, Phys. Rev. A **97**, 013851 (2018).
[41] C. L. Degen, F. Reinhard, and P. Cappellaro, Rev. Mod. Phys. **89**, 035002 (2017).
[42] J. Flick, M. Ruggenthaler, H. Appel, and A. Rubio, Proc. Natl. Acad. Sci. U.S.A. **114**, 3026 (2017).
[43] D. A. Steck, Rubidium 87 D line data, 2001, available at https://www.steck.us/alkalidata/rubidium87numbers.pdf
[44] E. V. Goldstein, P. Pax, and P. Meystre, Phys. Rev. A **53**, 2604 (1996).
[45] E. V. Goldstein and P. Meystre, Phys. Rev. A **56**, 5135 (1997).
[46] J. Guo and J. Cooper, Phys. Rev. A **51**, 3128 (1995).
[47] G. K. Brennen, I. H. Deutsch, and P. S. Jessen, Phys. Rev. A **61**, 062309 (2000).
[48] A. B. Klimov and L. L. Sanchez-Soto, Phys. Rev. A **61**, 063802 (2000).
[49] H. Breuer and F. Petruccione, *The Theory of Open Quantum Systems* (Oxford University Press, Oxford, 2002).
[50] C. Gardiner and P. Zoller, *Quantum Noise: A Handbook of Markovian and Non-Markovian Quantum Stochastic Methods with Applications to Quantum Optics*, Springer Series in Synergetics Vol. 56 (Springer Science + Business Media, New York, 2004).

[51] J. Klinder, H. Keßler, M. Wolke, L. Mathey, and A. Hemmerich, Proc. Natl. Acad. Sci. U.S.A. **112**, 3290 (2015).
[52] M. Premaratne and G. P. Agrawal, *Light Propagation in Gain Media: Optical Amplifiers* (Cambridge University Press, Cambridge, 2011).
[53] M. J. Bhaseen, J. Mayoh, B. D. Simons, and J. Keeling, Phys. Rev. A **85**, 013817 (2012).
[54] D. Kruse, M. Ruder, J. Benhelm, C. von Cube, C. Zimmermann, P. W. Courteille, T. Elsässer, B. Nagorny, and A. Hemmerich, Phys. Rev. A **67**, 051802(R) (2003).
[55] H. Hapuarachchi, M. Premaratne, Q. Bao, W. Cheng, S. D. Gunapala, and G. P. Agrawal, Phys. Rev. B **95**, 245419 (2017).
[56] Y. K. Wang and F. Hioe, Phys. Rev. A **7**, 831 (1973).
[57] F. D. De Oliveira, Study of the Dicke model: From phase space approach to quantum trajectories, Ph.D. thesis, University of Auckland, 2008.
[58] C. Emary and T. Brandes, Phys. Rev. E **67**, 066203 (2003).
[59] T. Brandes, Phys. Rep. **408**, 315 (2005).
[60] Y. Todorov and C. Sirtori, Phys. Rev. X **4**, 041031 (2014).
[61] Y. Todorov, A. M. Andrews, R. Colombelli, S. De Liberato, C. Ciuti, P. Klang, G. Strasser, and C. Sirtori, Phys. Rev. Lett. **105**, 196402 (2010).
[62] D. Walls and G. J. Milburn, *Quantum Optics* (Springer, Berlin, 2008).
[63] T. Mansour and M. Schork, Russ. J. Math. Phys. **15**, 77 (2008).
[64] R. J. Glauber, Phys. Rev. **131**, 2766 (1963).
[65] E. Sudarshan, Phys. Rev. Lett. **10**, 277 (1963).
[66] P. Drummond and C. Gardiner, J. Phys. A: Math. Gen. **13**, 2353 (1980).
[67] H. J. Carmichael and M. O. Scully, Phys. Today **53**(3), 78 (2000).
[68] B. Dayan, A. Parkins, T. Aoki, E. Ostby, K. Vahala, and H. Kimble, Science **319**, 1062 (2008).
[69] S. M. Spillane, T. J. Kippenberg, K. J. Vahala, K. W. Goh, E. Wilcut, and H. J. Kimble, Phys. Rev. A **71**, 013817 (2005).
[70] S. Barnett and P. M. Radmore, *Methods in Theoretical Quantum Optics* (Oxford University Press, Oxford, 2002), Vol. 15.
[71] M. Hillery, R. F. O'Connell, M. O. Scully, and E. P. Wigner, Phys. Rep. **106**, 121 (1984).
[72] S. Sachdev, *Handbook of Magnetism and Advanced Magnetic Materials* (Wiley, New York, 2007).
[73] P. Calabrese and J. Cardy, Int. J. Quantum Inf. **4**, 429 (2006).
[74] M. B. Plenio and S. S. Virmani, in *Quantum Information and Coherence*, edited by E. Andersson and P. Öhberg (Springer International, Cham, 2014), pp. 173–209.
[75] G. Vidal and R. F. Werner, Phys. Rev. A **65**, 032314 (2002).
[76] D. Lv, S. An, Z. Liu, J.-N. Zhang, J. S. Pedernales, L. Lamata, E. Solano, and K. Kim, Phys. Rev. X **8**, 021027 (2018).
[77] E. Hagley, X. Maitre, G. Nogues, C. Wunderlich, M. Brune, J.-M. Raimond, and S. Haroche, Phys. Rev. Lett. **79**, 1 (1997).